AFRL-VS-HA-TR-1998-0087

ERROR ANALYSIS OF PADDING SCHEMES FOR DFT'S OF CONVOLUTIONS AND DERIVATIVES

Christopher Jekeli

Ohio State University
Department of Civil and Environmental Engineering
and Geodetic Science
2070 Neil Ave.
Columbus, OH 43210

14 September 1998

Final Report

AIR FORCE RESEARCH LABORATORY
Space Vehicles Directorate
29 Randolph Rd
AIR FORCE MATERIEL COMMAND
HANSCOM AFB, MA 01731-3010

This technical report has been reviewed and is approved for publication

(Signature)
Anestis J. Romaides
Contract Manager

(Signature)
Mark P. Wilson, Major, USAF
Space Weather Effects Team Lead

(Signature)
Gregory P. Ginet, Chief
Space Weather Center of Excellence

This report has been reviewed by the ESC Public Affaires Office (PA) and is releasable to the National Technical Information Service (NTIS).

Qualified requestors may obtain additional copies from the Defense Technical Information Center (DTIC). All others should apply to the National Technical Information Service (NTIS).

If your address has changed, if you wish to be removed from the mailing list, or if the addressee is no longer employed by your organization, please notify AFRL/VSIM, 29 Randolph Road, Hanscom AFB, MA 01731-3010. This will assist us in maintaining a current mailing list.

Do not return copies of this report unless contractual obligations or notices on a specific document require that it be returned.

REPORT DOCUMENTATION PAGE

Form Approved OMB No. 0704-0188

1. REPORT DATE *(DD-MM-YYYY)*	2. REPORT TYPE	3. DATES COVERED *(From - To)*
September 1998	Scientific, final	September 1994 – September 1998

4. TITLE AND SUBTITLE
Error Analysis of Padding Schemes for DFT's of Convolutions and Derivatives

5a. CONTRACT NUMBER
F19628-94-K-0005

5b. GRANT NUMBER

5c. PROGRAM ELEMENT NUMBER

6. AUTHOR(S)
Christopher Jekeli

5d. PROJECT NUMBER
DMAP

5e. TASK NUMBER
GL

5f. WORK UNIT NUMBER
AA

7. PERFORMING ORGANIZATION NAME(S) AND ADDRESS(ES)
Department of Civil and Environmental Engineering and Geodetic Science
Ohio State University
2070 Neil Ave.
Columbus, OH 43210-1275

8. PERFORMING ORGANIZATION REPORT NUMBER
Report No. 446

9. SPONSORING / MONITORING AGENCY NAME(S) AND ADDRESS(ES)
Air Force Research Laboratory/VSBI
29 Randolph Rd.
Hanscom AFB, MA 01731-3010

10. SPONSOR/MONITOR'S ACRONYM(S)

11. SPONSOR/MONITOR'S REPORT NUMBER(S)
AFRL-VS-HA-TR-98-0087

12. DISTRIBUTION / AVAILABILITY STATEMENT
Approved for Public Release; Distribution unlimited

13. SUPPLEMENTARY NOTES

14. ABSTRACT

Various padding schemes have been proposed in the geodetic literature to avoid the error committed by approximating a linear convolution with a cyclic convolution; the latter is needed to implement Fast Fourier transform techniques. The method of extending the signal with zeros and the kernel with its own values yields equality between the two types of convolutions. However, it is shown using error transfer functions and numerical examples that the cyclic convolution error is not greater than the edge effect. Since the edge effect must be avoided in any case, there is justification for dispensing with the padding of arrays that adds considerably to computer memory requirements. The analysis is extended to the method of properly defined discrete, derivative operator transforms where the corresponding cyclic convolution error is confined to computation points very close to the edge.

15. SUBJECT TERMS
Circular Convolution, Discrete Fourier Transform, Geodetic Convolutions, Edge Effect

16. SECURITY CLASSIFICATION OF:			17. LIMITATION OF ABSTRACT	18. NUMBER OF PAGES	19a. NAME OF RESPONSIBLE PERSON
a. REPORT	b. ABSTRACT	c. THIS PAGE	SAR		19b. TELEPHONE NUMBER *(include area code)*
UNCLASSIFIED	UNCLASSIFIED	UNCLASSIFIED			

Table of Contents

List of Illustrations

1. Introduction

In physical geodesy, the determination of various quantities, like the geoid undulation, the deflection of the vertical, the terrain correction, and similar quantities attributable to mass attraction, involve the calculation of convolution integrals. In these applications, one may call the two functions being convolved the *signal function* (or *data*) and the *kernel function*, where the latter represents the model, or system, that transforms the data in some physically meaningful way. For example, Stokes' formula is a convolution of gravity anomalies (the data) with Stokes' function (the kernel) that produces the geoid undulation. Although these convolutions are of functions on the sphere, only planar approximations will be considered here.

It is well known that, because the data that enter the convolution are finite and discrete and because certain fast computational techniques require it, the convolution theoretically defined on the entire plane must be replaced with a convolution for periodic functions. This use of the so-called circular convolution, instead of the linear convolution, therefore, naturally introduces corresponding errors in the model for the desired quantity.

There are two basic approaches to treating this error that have been used in the past. The first simply ignores the error. This was the case, for example, in Schwarz et al. (1990); and it has justification, as will be seen. The second approach is based on extending the finite, discrete data arrays being convolved with zeros. This artifice was discussed by Oppenheim and Schafer (1975). Many numerical tests have been done to show that this so-called zero padding improves the computation of Stokes' integral in planar approximation using the discrete Fourier transform (or, equivalently, the fast Fourier transform, FFT); one may cite Tziavos (1992), Sideris and Li (1993), and Haagmans et al. (1993). Furthermore, several padding variations have been investigated numerically, including the extension (padding) of both the data and kernel with zeros (Zhang, 1995), the extension of the data with zeros and the kernel with its known values (Sideris and Li, 1993), as well as the tapering of the data in a border to zero at the edges (Vermeer, 1995; Tziavos, 1996). It is clear from this recent geodetic literature that there remains some confusion as to the nature and appropriateness of the padding schemes and the relationship between the linear and circular convolutions. It is noted that Haagmans et al. (1993) make the clearest statement that the correct padding scheme is one where only the data are extended with zeros and the kernel is naturally extended. However, they give only a graphical "proof".

The purpose of this report is to analyze the padding schemes that do not yield equality between the circular and linear convolutions, and to determine the quantitative relationship between the circular convolution error and the edge effect. Explicit formulas for the errors in the padding schemes and for the edge effect are derived; and these errors are then analyzed using transfer functions and a numerical example. The analysis proceeds to properly defined frequency responses of discrete derivative operators, including those that are applied to convolutions. The

mathematical derivations are restricted to a single dimension in order to maximize simplicity. The results can easily be generalized by inference to higher dimensions and are given explicitly for two dimensions.

2. Convolutions

Three types of convolution will be needed. The first is for continuous functions defined over the real line. Let g(t) and h(t) be two functions, where t is a real number. Their (linear) convolution is denoted by $(g * h)(t)$ and is given by

$$(g * h)(t) = \int_{-\infty}^{\infty} g(\tau)\, h(t-\tau)\, d\tau \ , \quad -\infty < t < \infty \tag{1}$$

It is assumed that, as $|t| \to \infty$, the functions g(t) and h(t) attenuate to zero in such a way that the convolution (1) exists for all t.

For discrete, infinite sequences, g_k and h_k, of presumably *evenly spaced samples* of these functions, the linear, discrete convolution is denoted by $(g \# h)_k$, and it is given by

$$(g \# h)_k = \sum_{n=-\infty}^{\infty} g_n\, h_{k-n} \ ; \quad k \in Z \tag{2}$$

where Z is the set of integers; and, again, it is assumed that the sum exists.

Finally, consider the periodic sequences, $\left(\tilde{g}_N\right)_k$ and $\left(\tilde{h}_N\right)_k$, each having the same period, N. The convolution as defined in (2) does not exist for these sequences, and an alternative definition is required. The *periodic* (or *cyclic*), *discrete convolution* is denoted by $\left(\tilde{g}_N \tilde{\#} \tilde{h}_N\right)_k$, and it is given by

$$\left(\tilde{g}_N \tilde{\#} \tilde{h}_N\right)_k = \sum_{n=-N/2}^{N/2-1} \left(\tilde{g}_N\right)_n \left(\tilde{h}_N\right)_{k-n} \ ; \quad -\frac{N}{2} \le k \le \frac{N}{2} - 1 \tag{3}$$

where, without loss of generality, one may assume that the integer N is even. Any consecutive set of integers n in the summation may be used because of the periodicity of the sequences. Of course, the convolution itself is also periodic with the same period, N.

The discrete Fourier transform (DFT) $\left(\tilde{g}_N\right)_k$ is defined by

$$\left(\tilde{G}_N\right)_\ell \equiv \mathrm{DFT}\left(\tilde{g}_N\right) = \sum_{k=0}^{N-1} \left(\tilde{g}_N\right)_k e^{-i\frac{2\pi}{N}k\ell} \quad ; \quad \ell = 0, \ldots, N-1 \tag{4}$$

Here, the more traditional index sequence, $k, \ell = 0, \ldots, N-1$, is used; however, because of the periodicity (also, of the exponentials), any other sequence of N indices yields an equivalent transform. Because $\left(\tilde{g}_N\right)_k$ is assumed to be a real-valued sequences, the DFT has the following conjugate-symmetry property, that can be proved easily from (4):

$$\left(\tilde{g}_N\right)_k \text{ is } \textit{real} \text{ for all } k \;\Leftrightarrow\; \left(\tilde{G}_N^*\right)_\ell = \left(\tilde{G}_N\right)_{N-\ell} \text{ for any } \ell \tag{5}$$

where superscript-* signifies complex conjugate.

3. Approximations

The continuous convolution (1) represents the reality (the model) of the operation that combines the data and kernel functions, g and h. In practice, one has a *finite* number of *discrete* values of the signal, that is, a finite sequence of N (equally spaced) data, g_k. If these data are given (again, without loss in generality) on the interval $-N/2 \le k \le N/2 - 1$, then the true convolution (1) may be broken into a number of parts:

$$\begin{aligned}\int_{-\infty}^{\infty} g(\tau)\, h(t-\tau)\, d\tau &= \int_{-T/2}^{T/2} g(\tau)\, h(t-\tau)\, d\tau + \int_{T/2<|\tau|<T/2+|t|} g(\tau)\, h(t-\tau)\, d\tau + \int_{T/2+|t|<|\tau|<\infty} g(\tau)\, h(t-\tau)\, d\tau \\ &= \left(g_T * h\right)(t) - \varepsilon_{\text{edge}} - \varepsilon_{\text{trunc}} \\ &= \left(g_N \# h\right)_k - \varepsilon_{\text{edge}} - \varepsilon_{\text{discret}} - \varepsilon_{\text{trunc}}\end{aligned} \tag{6}$$

where T is the corresponding continuous interval on the real line (if Δt is the sampling interval, then $T = N\,\Delta t$), and where the *function*, $g_T(t)$, is given by

$$g_T(t) = \begin{cases} g(t), & -\frac{T}{2} \le t \le \frac{T}{2} \\ 0, & \text{otherwise} \end{cases} \tag{7}$$

The truncated sequence, $(g_N)_k$, represents the collection of available samples of the signal, i.e., the data:

$$(g_N)_k = \begin{cases} g_k, & -\frac{N}{2} \le k \le \frac{N}{2} - 1 \\ 0, & \text{otherwise} \end{cases} \tag{8}$$

The first part of the final equation in (6), the discrete convolution, can be calculated from the data, while the second, third, and fourth parts, ε_{edge}, $\varepsilon_{discret}$, ε_{trunc}, represent errors, called, respectively, the *edge effect*, the *discretization error*, and the *truncation error* (see Figure 1).

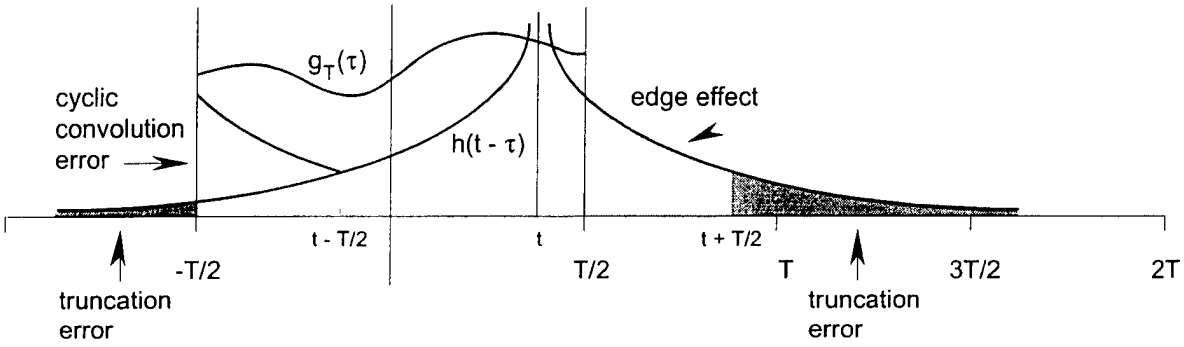

Figure 1: Truncation error and edge effect for the convolution $(g_T * h)(t)$. Also shown for later reference is the cyclic convolution error.

The edge effect and truncation error are due to the finite extent of the data, but the edge effect is considered separately since it can be avoided to some extent by limiting the domain of t to an interval smaller than the data interval (it is zero, when $t = 0$). Neither the discretization error nor the remaining truncation error is within the scope of this discussion. Both can be reduced to acceptable levels with sufficient sampling in density and extent. Instead, the error in computing the convolution by DFT is now investigated. It is assumed that the kernel function, h, is known for all t; therefore, it can be sampled for all k.

In order to use the DFT (or, FFT), one must assume that both the data and the kernel sequences are periodic. Thus, to proceed, consider the following assignments:

$$(\tilde{g}_N)_k = g_k, \quad (\tilde{g}_N)_{k+\ell N} = g_k, \quad -\frac{N}{2} \le k \le \frac{N}{2} - 1, \quad \ell \in Z \tag{9}$$

$$(\tilde{h}_N)_k = h_k, \quad (\tilde{h}_N)_{k+\ell N} = h_k, \quad -\frac{N}{2} \le k \le \frac{N}{2} - 1, \quad \ell \in Z \tag{10}$$

Then, the *linear*, discrete convolution in (6) should be approximated by a *cyclic*, discrete convolution. There are the following alternatives, in each for $-N/2 \le k \le N/2 - 1$:

$$(g_N \# h)_k = (\tilde{g}_N \tilde{\#} \tilde{h}_N)_k - (\varepsilon_1)_k \tag{11}$$

$$(g_N \# h)_k = (\tilde{g}^0_{2N} \tilde{\#} \tilde{h}^0_{2N})_k - (\varepsilon_2)_k \tag{12}$$

$$(g_N \# h)_k = (\tilde{g}^0_{2N} \tilde{\#} \tilde{h}_{2N})_k - (\varepsilon_3)_k \tag{13}$$

where $\tilde{g}^0_{2N}$ (similarly, $\tilde{h}^0_{2N}$) is a periodic sequence defined by the extension of $\tilde{g}_N$ with zeros on either side for an interval equal to half the length of the original sequence:

$$(\tilde{g}^0_{2N})_k = \begin{cases} g_k, & -\frac{N}{2} \le k \le \frac{N}{2} - 1 \\ 0, & -N \le k \le -\frac{N}{2} - 1 \text{ and } \frac{N}{2} \le k \le N - 1 \end{cases}$$

$$(\tilde{g}^0_{2N})_{k+2\ell N} = (\tilde{g}^0_{2N})_k, \quad -N \le k \le N-1, \ \ell \in Z \tag{14}$$

Also, the extended periodic sequence $\tilde{h}_{2N}$ is defined by

$$(\tilde{h}_{2N})_k = h_k, \quad (\tilde{h}_{2N})_{k+2\ell N} = (\tilde{h}_{2N})_k, \quad -N \le k \le N-1, \ \ell \in Z \tag{15}$$

The first approximation (11) appears in the early geodetic literature dealing with Fourier techniques (e.g., Schwarz et al., 1990). Equation (12) was considered by some as a way to reduce the circular convolution effects through zero-padding of both data and kernel functions. The third possibility, (13), reflects the case where the data are extended with zeros, but the kernel sequence, though assumed periodic (period 2N), is extended naturally using its own values. Elaborating on this case, it is easy to prove that $\varepsilon_3 = 0$. First note that

$$(\tilde{g}^0_{2N})_n = (g_N)_n \ ; \quad -N \le n \le N-1 \tag{16}$$

$$(\tilde{h}_{2N})_{k-n} = (h_{2N})_{k-n} = h_{k-n} \ ; \quad -\frac{N}{2} \le n \le \frac{N}{2} - 1 \text{ and } -\frac{N}{2} \le k \le \frac{N}{2} - 1 \tag{17}$$

Therefore we have, for $-N/2 \le k \le N/2 - 1$:

$$\left(\tilde{\tilde{g}}^{0}_{2N} \tilde{\#} \tilde{h}_{2N}\right)_k = \sum_{n=-N}^{N-1} (g_N)_n \left(\tilde{h}_{2N}\right)_{k-n} \quad ; \qquad \text{from (3) and (16)}$$

$$= \sum_{n=-N/2}^{N/2-1} (g_N)_n \, h_{k-n} \quad ; \qquad \text{from (8) and (17)}$$

Hence, from (8) and the definition of discrete convolution (2),

$$\left(g_N \# h\right)_k = \left(\tilde{\tilde{g}}^{0}_{2N} \tilde{\#} \tilde{h}_{2N}\right)_k \quad ; \qquad -\frac{N}{2} \le k \le \frac{N}{2} - 1 \tag{18}$$

showing that $\varepsilon_3 = 0$, i.e., that the cyclic convolution of the zero-padded data and the naturally extended kernel sequences equals the linear convolution of the original sequences.

This result can be specialized immediately to the case where the *kernel* sequence is also padded with zeros (like $\tilde{\tilde{g}}^{0}_{2N}$ in (14)), because the natural extension of h_N is $\tilde{h}^{0}_{2N}$:

$$\left(g_N \# h_N\right)_k = \left(\tilde{\tilde{g}}^{0}_{2N} \tilde{\#} \tilde{h}^{0}_{2N}\right)_k \quad ; \qquad -\frac{N}{2} \le k \le \frac{N}{2} - 1 \tag{19}$$

Both equations (18) and (19) relate linear convolutions to corresponding cyclic convolutions. Equation (19) is the justification, originating in Oppenheim and Schafer (1975), for padding both sequences with zeros over appended intervals on either side equal in length to N/2. But this is the correct procedure *only if* both sequences are available only over the truncated interval $-N/2 \le k \le N/2 - 1$. It is clear from (6) that, since we know the function h (it need not be truncated), the proper cyclic convolution to be used is (18), *not* (19).

It can be shown with due consideration of the sequence definitions, that the errors associated with the alternatives (11) and (12) are given, respectively, by

$$\left(\varepsilon_1\right)_k = \begin{cases} \displaystyle\sum_{n=k+N/2+1}^{N/2-1} g_n \left(h_{k-n+N} - h_{k-n}\right), & -\frac{N}{2} \le k \le -2 \\ 0 & k = -1 \\ \displaystyle\sum_{n=-N/2}^{-N/2+k} g_n \left(h_{k-n-N} - h_{k-n}\right), & 0 \le k \le \frac{N}{2} - 1 \end{cases} \tag{20}$$

and

$$(\varepsilon_2)_k = \begin{cases} -\sum_{n=k+N/2+1}^{N/2-1} g_n h_{k-n}, & -\frac{N}{2} \le k \le -2 \\ 0 & k = -1 \\ -\sum_{n=-N/2}^{-N/2+k} g_n h_{k-n}, & 0 \le k \le \frac{N}{2} - 1 \end{cases} \tag{21}$$

The fact that the errors in these cases are zero at $k = -1$ instead of $k = 0$ is an artifact of N being even. Note that the summand in $(\varepsilon_1)_k$ (see Figure 1) involves the values of the kernel function potentially close to the origin, while for $(\varepsilon_2)_k$, only the tail ends of h enter. Hence, if the kernel is largest near the origin and attenuates with distance from the origin (many geodetic kernels, in fact, behave like the reciprocal distance), then the error $(\varepsilon_1)_k$ is generally much larger than $(\varepsilon_2)_k$. Of course, this comparison is almost irrelevant if alternative (18) is used. However, each method differs in the computational load and computer memory requirements, and these may be important considerations.

4. Edge Effect

The edge effect error, for $0 < t < T/2$, is given by

$$\varepsilon_{edge}(t) = -\int_{T/2}^{T/2+t} g(\tau)\, h(t-\tau)\, d\tau \tag{22}$$

with a similar integral for $-T/2 < t < 0$. An approximation is a discretization of this, again, for $0 \le k < N/2 - 1$:

$$(\varepsilon_{edge})_k = -\sum_{n=N/2}^{N/2+k} g_n h_{k-n} \tag{23}$$

and a similar expression for $-N/2 \le k \le -2$. The edge effect is zero for $k = -1$. It is already clear from Figure 1 that $(\varepsilon_{edge})_k$ and $(\varepsilon_1)_k$ have commensurate error characteristics.

Figure 2 shows that the edge effect and truncation error remain unchanged with the introduction of the extended sequence $\tilde{g}^{0}_{2N}$. The cyclic convolution error in this case is zero (as shown in (18)) because the extended, periodic kernel function multiplies only zeros in the extended data sequence.

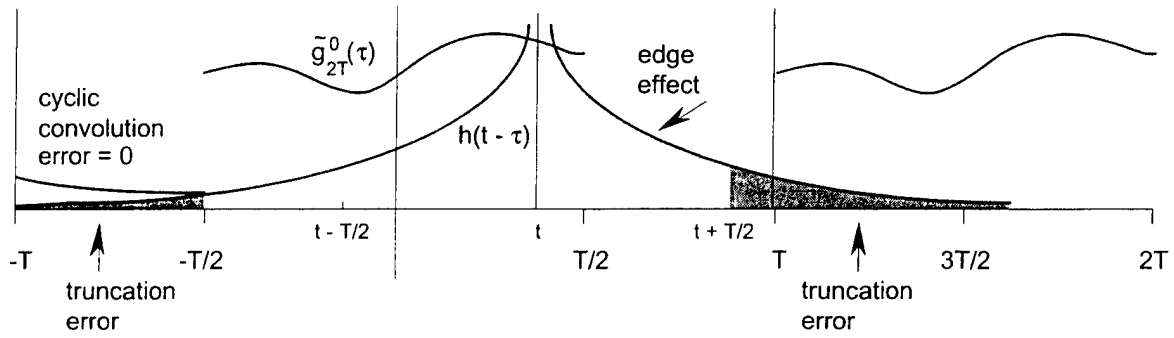

Figure 2: Truncation error, edge effect, and cyclic convolution error for the extended, zero-padded data sequence.

5. Extension to Two Dimensions

The derivations of the previous section for one-dimensional functions and sequences can easily be extended to two dimensions, if the coordinates are Cartesian. The appropriate cyclic convolution to use in place of the linear convolution, from (18), is formally given by

$$\left(g_{N_1,N_2} \# h\right)_{k_1,k_2} = \left(\tilde{g}^{0,0}_{2N_1,2N_2} \tilde{\#} \tilde{h}_{2N_1,2N_2}\right)_{k_1,k_2} ; \quad -\frac{N_1}{2} \le k_1 \le \frac{N_1}{2} - 1 \ , \ -\frac{N_2}{2} \le k_2 \le \frac{N_2}{2} - 1 \tag{24}$$

where

$$\left(\tilde{g}^{0,0}_{2N_1,2N_2}\right)_{k_1,k_2} = \begin{cases} \left(\tilde{g}_{N_1,N_2}\right)_{k_1,k_2}, & -\frac{N_1}{2} \le k_1 \le \frac{N_1}{2} - 1 \text{ and } -\frac{N_2}{2} \le k_2 \le \frac{N_2}{2} - 1 \\ 0, & -N_1 \le k_1 \le -\frac{N_1}{2} - 1 \text{ or } \frac{N_1}{2} \le k_1 \le N_1 - 1 \text{ or} \\ & -N_2 \le k_2 \le -\frac{N_2}{2} - 1 \text{ or } \frac{N_2}{2} \le k_2 \le N_2 - 1 \end{cases}$$

$$\left(\tilde{g}^{0,0}_{2N_1,2N_2}\right)_{k_1 + 2\ell_1 N_1, k_2 + 2\ell_2 N_2} = \left(\tilde{g}^{0,0}_{2N_1,2N_2}\right)_{k_1,k_2} , \quad -N_1 \le k_1 \le N_1 - 1 , \ -N_2 \le k_2 \le N_2 - 1 , \ \ell_1,\ell_2 \in Z \tag{25}$$

That is, the zero-padded signal array, $\tilde{g}^{0,0}_{2N_1,2N_2}$, is the original array plus a border of zeros, whose width is either $(N_1)/2$ or $(N_2)/2$, depending on the coordinate direction. This extended array is continued periodically over the entire plane. The periodic kernel array is defined analogous to (15):

$$\left(\tilde{h}_{2N_1,2N_2}\right)_{k_1,k_2} = h_{k_1,k_2}, \qquad -N_1 \le k_1 \le N_1 - 1\ ,\ \ -N_2 \le k_2 \le N_2 - 1$$

$$\left(\tilde{h}_{2N_1,2N_2}\right)_{k_1+2\ell_1 N_1,\,k_2+2\ell_2 N_2} = \left(\tilde{h}_{2N_1,2N_2}\right)_{k_1,k_2}, \quad \ell_1, \ell_2 \in Z \tag{26}$$

where the extension to the larger $2N_1 \times 2N_2$ grid is accomplished using the actual values of the kernel function.

6. Alternative Indexing

Most FFT algorithms assume the DFT is defined with indices starting at zero, as in (4). Because of its periodicity, the cyclic convolution that is identical to the linear convolution still is Eq. (23). The difference is in the padding of the extended kernel array prior to convolution. In essence, the padding scheme is no different than what is specified by (26), but by shifting the index to start at zero, the extended part of the array is *not* filled with the natural values of h, but by the values of h for negative indices. That is, we simply use an interval of the domain of $\tilde{h}_{2N_1,2N_2}$ other than the principal one given in (26), that happens to start at (0,0).

One has the following algorithm for padding the data and the kernel, respectively:

$$\left(\tilde{g}_{2N_1,2N_2}\right)_{k_1,k_2} = \begin{cases} g_{k_1,k_2}, & 0 \le k_1 \le N_1 - 1, \quad 0 \le k_2 \le N_2 - 1 \\ 0 & N_1 \le k_1 \le 2N_1 - 1, \quad 0 \le k_2 \le N_2 - 1 \\ 0 & 0 \le k_1 \le N_1 - 1, \quad N_2 \le k_2 \le 2N_2 - 1 \\ 0 & N_1 \le k_1 \le 2N_1 - 1, \quad N_2 \le k_2 \le 2N_2 - 1 \end{cases} \tag{27}$$

$$\left(\tilde{h}_{2N_1,2N_2}\right)_{k_1,k_2} = \begin{cases} h_{k_1,k_2}, & 0 \le k_1 \le N_1 - 1, \quad 0 \le k_2 \le N_2 - 1 \\ h_{k_1-2N_1,k_2}, & N_1 \le k_1 \le 2N_1 - 1, \quad 0 \le k_2 \le N_2 - 1 \\ h_{k_1,k_2-2N_2}, & 0 \le k_1 \le N_1 - 1, \quad N_2 \le k_2 \le 2N_2 - 1 \\ h_{k_1-2N_1,k_2-2N_2}, & N_1 \le k_1 \le 2N_1 - 1, \quad N_2 \le k_2 \le 2N_2 - 1 \end{cases} \tag{28}$$

7. Error Analysis Equations

While it is easy to justify mathematically that (24) should always be used to compute the linear convolution (with zero error), the tax on computer memory and time may be prohibitive for very

large arrays (although, computer memory and processing speeds are still increasing at near exponential rates). For this reason it is instructive to study the errors associated with the use of the approximation corresponding to (11):

$$\left(g_{N_1,N_2} \# h\right)_{k_1,k_2} = \left(\tilde{g}_{N_1,N_2} \tilde{\#} \tilde{h}_{N_1,N_2}\right)_{k_1,k_2} - (\varepsilon_1)_{k_1,k_2}\,; \quad -\frac{N_1}{2} \le k_1 \le \frac{N_1}{2} - 1\,, \quad -\frac{N_2}{2} \le k_2 \le \frac{N_2}{2} - 1 \tag{29}$$

And, though it yields no savings in computer memory, the use of zero-padded kernels does offer some savings in computational time (for dimensions greater than 1, only), since the computation of DFT's of zero-vectors in the padded array is trivial. Thus, also the second approximation may be considered, corresponding to (12):

$$\left(g_{N_1,N_2} \# h\right)_{k_1,k_2} = \left(\tilde{g}^{0,0}_{N_1,N_2} \tilde{\#} \tilde{h}^{0,0}_{N_1,N_2}\right)_{k_1,k_2} - (\varepsilon_2)_{k_1,k_2}\,; \quad -\frac{N_1}{2} \le k_1 \le \frac{N_1}{2} - 1\,, \quad -\frac{N_2}{2} \le k_2 \le \frac{N_2}{2} - 1 \tag{30}$$

In the following, the errors $(\varepsilon_1)_{k_1,k_2}$ and $(\varepsilon_2)_{k_1,k_2}$, as well as the edge effect, are characterized in terms of their transfer functions - how they affect the convolution in terms of signal frequency.

Explicit expressions for these errors are analogous to equations (20), (21), and (23). However, in two dimensions, nine, instead of three, different expression are obtained, depending on the domain of (k_1,k_2). In addition, there are up to three summations over different ranges for each subdomain of (k_1,k_2). To simplify the notation, the following generalized expression is used:

$$\varepsilon_{k_1,k_2} = \sum_{n_1,n_2} g_{n_1,n_2}\, u_{k_1-n_1,k_2-n_2} \tag{31}$$

where the sum, Σ, represents a collection of sums, each over two indices of possibly different ranges; and where $u_{k_1-n_1,k_2-n_2}$ depends on values of the kernel function, as follows:

$$(\varepsilon_1)_{k_1,k_2}: \quad (u_1)_{k_1-n_1,k_2-n_2} = h_{k_1-n_1+a_1,k_2-n_2+a_2} - h_{k_1-n_1,k_2-n_2} \tag{32}$$

$$(\varepsilon_2)_{k_1,k_2}: \quad (u_2)_{k_1-n_1,k_2-n_2} = -h_{k_1-n_1,k_2-n_2} \tag{33}$$

$$(\varepsilon_{edge})_{k_1,k_2}: \quad (u_{edge})_{k_1-n_1,k_2-n_2} = -h_{k_1-n_1,k_2-n_2} \tag{34}$$

In Table 1, the ranges of (n_1, n_2) are listed for a partial set of the possible domains for (k_1,k_2) in the case of cyclic convolution errors, Eqs. (32) and (33). Similar index ranges can be derived for the other domains of (k_1,k_2), but one may limit the further discussions to those listed if the kernel

function is symmetric or antisymmetric (as it is in geodetic applications). Table 2 lists corresponding ranges of indices for the edge effect (34).

Table 1: Ranges of indices, (n_1, n_2), and values of a_1, a_2 (in (32)), for sums of (32) and (33) entering in equation (31). Domains $-N_1/2 \le k_1 \le -2$ and $-N_2/2 \le k_2 \le -2$ are omitted.

	$k_2 = -1$	$0 \le k_2 \le \frac{N_2}{2} - 1$
$k_1 = -1$	$(\varepsilon_1)_{-1,-1,} = 0$	$-\frac{N_1}{2} \le n_1 \le \frac{N_1}{2} - 1$ $-\frac{N_2}{2} \le n_2 \le -\frac{N_2}{2} + k_2$ | $a_1 = 0$ $a_2 = -N_2$
$0 \le k_1 \le \frac{N_1}{2} - 1$	$-\frac{N_1}{2} \le n_1 \le -\frac{N_1}{2} + k_1$ $-\frac{N_2}{2} \le n_2 \le \frac{N_2}{2} - 1$ | $a_1 = -N_1$ $a_2 = 0$	$-\frac{N_1}{2} \le n_1 \le -\frac{N_1}{2} + k_1$ $-\frac{N_2}{2} + k_2 + 1 \le n_2 \le \frac{N_2}{2} - 1$ | $a_1 = -N_1$ $a_2 = 0$
		$-\frac{N_1}{2} + k_1 + 1 \le n_1 \le \frac{N_1}{2} - 1$ $-\frac{N_2}{2} \le n_2 \le -\frac{N_2}{2} + k_2$ | $a_1 = 0$ $a_2 = -N_2$

It is now assumed that the signal is a stationary, stochastic process on the plane with zero mean. Using the notation in (31), the variance of the error ε_{k_1,k_2} is then given by

$$\sigma^2_{k_1,k_2} = E\left[\varepsilon^2_{k_1,k_2}\right]$$

$$= \sum_{n_1, n_2} \sum_{n_1', n_2'} u_{k_1 - n_1, k_2 - n_2} \, u_{k_1 - n_1', k_2 - n_2'} \, E\left[g_{n_1,n_2} \, g_{n_1',n_2'}\right] \tag{35}$$

where $E[\cdot]$ is the statistical expectation operator.

Table 2: Ranges of indices, (n_1, n_2), for sums of (34) entering in equation (31). Domains $-N_1/2 \le k_1 \le -2$ and $-N_2/2 \le k_2 \le -2$ are omitted.

	$k_2 = -1$	$0 \le k_2 \le \frac{N_2}{2} - 1$
$k_1 = -1$	$(\varepsilon_{edge})_{-1,-1} = 0$	$-\frac{N_1}{2} \le n_1 \le \frac{N_1}{2} - 1$ $\frac{N_2}{2} \le n_2 \le \frac{N_2}{2} + k_2$
$0 \le k_1 \le \frac{N_1}{2} - 1$	$\frac{N_1}{2} \le n_1 \le \frac{N_1}{2} + k_1$ $-\frac{N_2}{2} \le n_2 \le \frac{N_2}{2} - 1$	$\frac{N_1}{2} \le n_1 \le \frac{N_1}{2} + k_1$ $-\frac{N_2}{2} + k_2 + 1 \le n_2 \le \frac{N_2}{2} - 1$ $-\frac{N_1}{2} + k_1 + 1 \le n_1 \le \frac{N_1}{2} - 1$ $\frac{N_2}{2} \le n_2 \le \frac{N_2}{2} + k_2$ $\frac{N_1}{2} \le n_1 \le \frac{N_1}{2} + k_1$ $\frac{N_2}{2} \le n_2 \le \frac{N_2}{2} + k_2$

$E\left[g_{n_1,n_2}\, g_{n_1',n_2'}\right]$ is the auto-covariance of the discrete signal, which is also the continuous-signal auto-covariance function sampled at the discrete points $(n_1 - n_1', n_2 - n_2')$. If $\phi_g(f_1,f_2)$ is the power spectral density of g, depending on spatial frequencies, f_1, f_2, then

$$E\left[g_{n_1,n_2}\, g_{n_1',n_2'}\right] = \int_{-\infty}^{\infty}\int \phi_g(f_1,f_2)\, e^{i\,2\pi\left[f_1(n_1 - n_1') + f_2(n_2 - n_2')\right]}\, df_1\, df_2 \tag{36}$$

Substituting this into (35) yields

$$\sigma^2_{k_1,k_2} = \int_{-\infty}^{\infty}\int U_{k_1,k_2}\, U^*_{k_1,k_2}\, \phi_g(f_1,f_2)\, df_1\, df_2 \tag{37}$$

where the "transfer function", U_{k_1,k_2}, is given by

$$U_{k_1,k_2}(f_1,f_2) = \sum_{n_1,n_2} u_{k_1 - n_1,k_2 - n_2}\, e^{i\,2\pi\left[f_1 n_1 + f_2 n_2\right]} \tag{38}$$

Note that the transfer function is not shift-invariant, but depends on the computation point

coordinates (k_1,k_2).

With suitable reorganization of indices, it is easily shown that

$$U_{k_1,k_2}(f_1,f_2)\,U^{*}_{k_1,k_2}(f_1,f_2) = \left|U_{k_1,k_2}(f_1,f_2)\right|^2$$

$$= \left[\sum_{k_1-n_1,k_2-n_2} u_{n_1,n_2}\cos\left[2\pi\left(f_1n_1+f_2n_2\right)\right]\right]^2 + \left[\sum_{k_1-n_1,k_2-n_2} u_{n_1,n_2}\sin\left[2\pi\left(f_1n_1+f_2n_2\right)\right]\right]^2 \tag{39}$$

8. Error Analysis Results

This section contains the numerical evaluation of the cyclic convolution error for the two most prevalent kernel functions in geodesy. These kernels are

$$h(x_1,x_2) = \frac{1}{\left(x_1^2+x_2^2\right)^{1/2}} \tag{40}$$

used in the computation of the geoid undulation from gravity anomalies (planar approximation to Stokes' function); and

$$h(x_1,x_2) = \frac{1}{\left(x_1^2+x_2^2\right)^{3/2}} \tag{41}$$

used in the computation of the vertical gradient of harmonic functions (upward/downward continuation in Molodensky's geodetic boundary value problem); it also appears in the terrain correction and other convolutions (again, always in planar approximation). To simplify the graphic depictions, the computation points are restricted to $k_1 = k_2 = k$; the frequencies are restricted to $f_1 = f_2 = f$; and, $N_1 = N_2 = N$.

Figures 3, 4, and 5 correspond to the geoid undulation kernel (40); while, Figures 6 and 7 correspond to the vertical gradient kernel (41). Each figure shows the magnitude of the error transfer function, $\left|U_{k,k}(f,f)\right|$, depending on the computation point $(k\Delta x,k\Delta x)$ and the frequency pair (f_j,f_j), where $f_j = j/(2N\Delta x)$, and N = 96. For other values of N one obtains similar plots, and the following discussion is meant to be more qualitative than quantitative.

Consider Figure 3, showing the transfer function for the cyclic convolution error, $(\varepsilon_1)_{k,k}$. Each vertical (frequency) profile of the function represents the transfer function of the error for a particular computation point of the convolution. Clearly, they are like low-pass filters, affecting primarily the lower frequencies of the signal. Also, as the computation point nears the edge of the signal area, the cyclic convolution error becomes larger, as expected. Nevertheless, if it is not too

close to the edge, the error may be acceptable. This is especially true for the kernel (41) (see Figure 6).

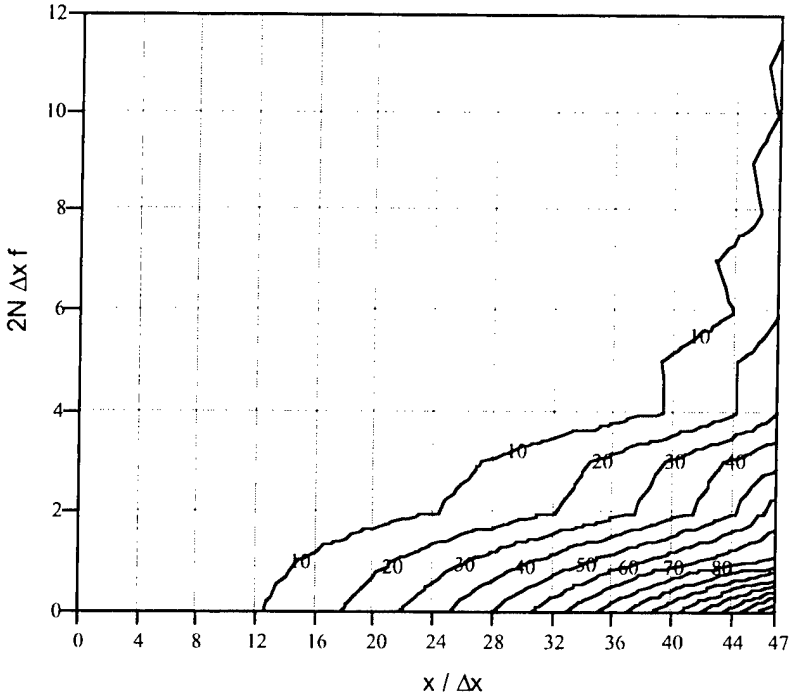

Figure 3. Transfer function of cyclic convolution error ε_1 for kernel (40).

There is also the interesting possibility with the kernel (40) (Figure 3) that if the signal has no low-frequency content then that same acceptable error occurs for computation points even closer to the edge. In the example of Figure 3, if $x = 12\,\Delta x$ represents the computation point at which the error transfer function is negligibly small for all frequencies of the signal, then $x = 39\,\Delta x$ is the computation point where the error is negligible if the signal has no frequency content below $f = 5/(192\,\Delta x)$.

Figure 4 shows the transfer function for the cyclic convolution error $(\varepsilon_2)_{k,k}$, caused by improperly padding the kernel function (40) with zeros. Such a procedure has the potential to reduce computation times, compared to the correct padding method; but as seen in the figure, it should only be used if the signal is high-pass filtered.

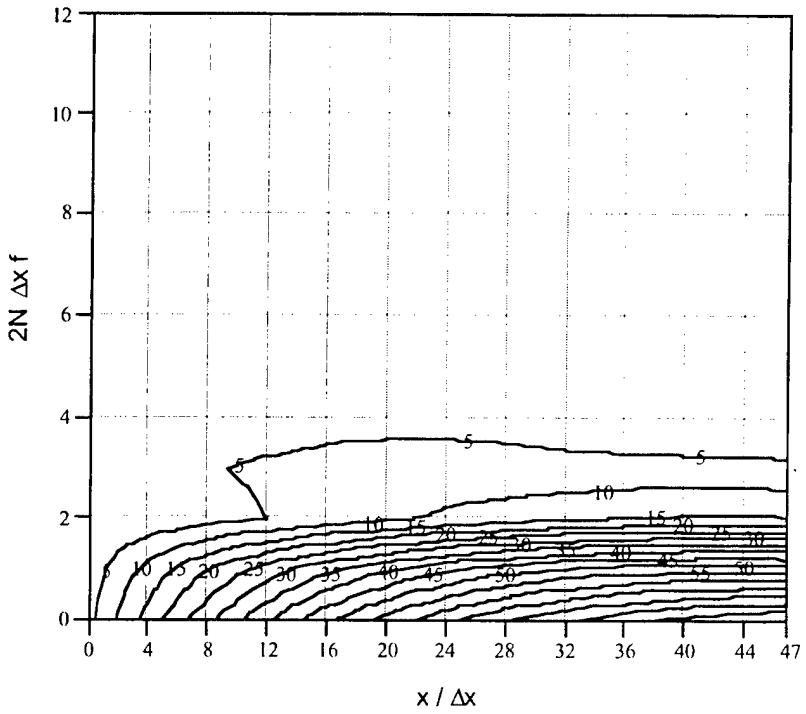

Figure 4. Transfer function of cyclic convolution error ε_2 for kernel (40).

Figure 5 verifies that the edge effect error and the cyclic convolution error, ε_1, have similar spectral characteristics, as evidenced by their transfer functions. Therefore, in avoiding the edge effect by restricting the computation point of the convolution to an interior subdomain of the signal area, one also avoids the cyclic convolution error, even if no zero-padding is performed.

Figures 6 and 7 show the analogous spectral transfer properties, respectively, of the circular convolution and edge effect errors for the kernel (41). Because this kernel is much narrower near the origin, the errors are strongest only for computation points very close to the edge of the signal area. Note the break in the abscissa scale in these figures and the similarity in the transfer functions.

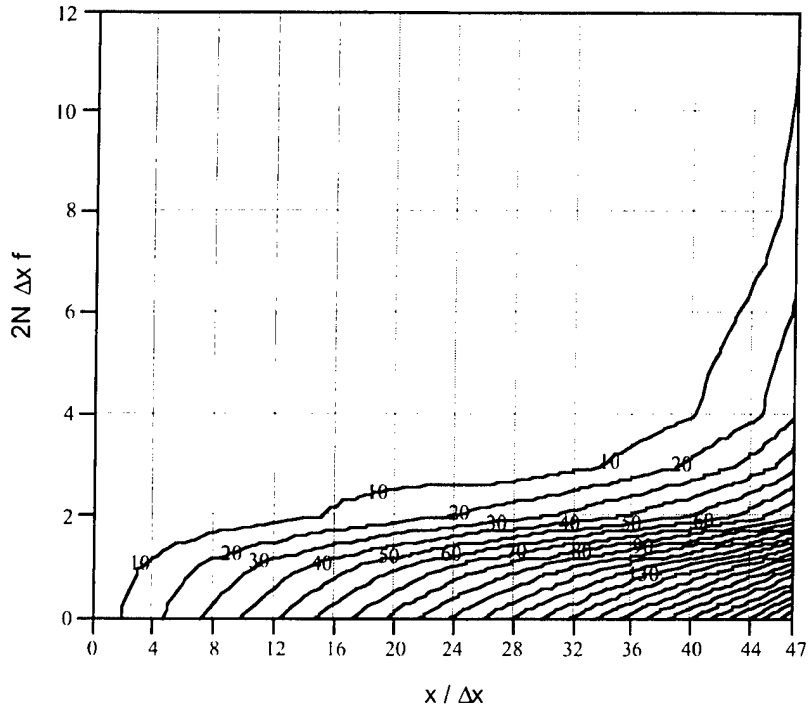

Figure 5. Transfer function of edge effect error for kernel (40).

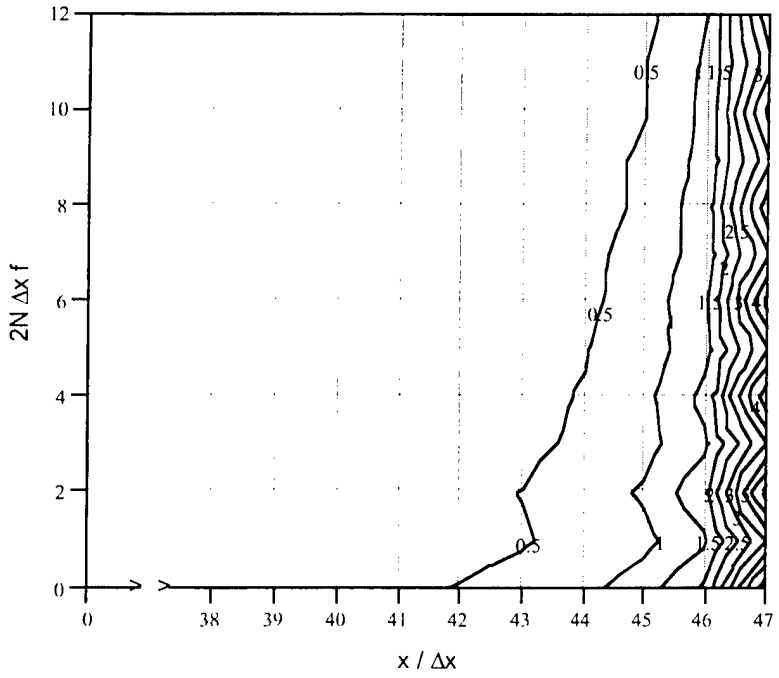

Figure 6. Transfer function of cyclic convolution error ε_1 for kernel (41).

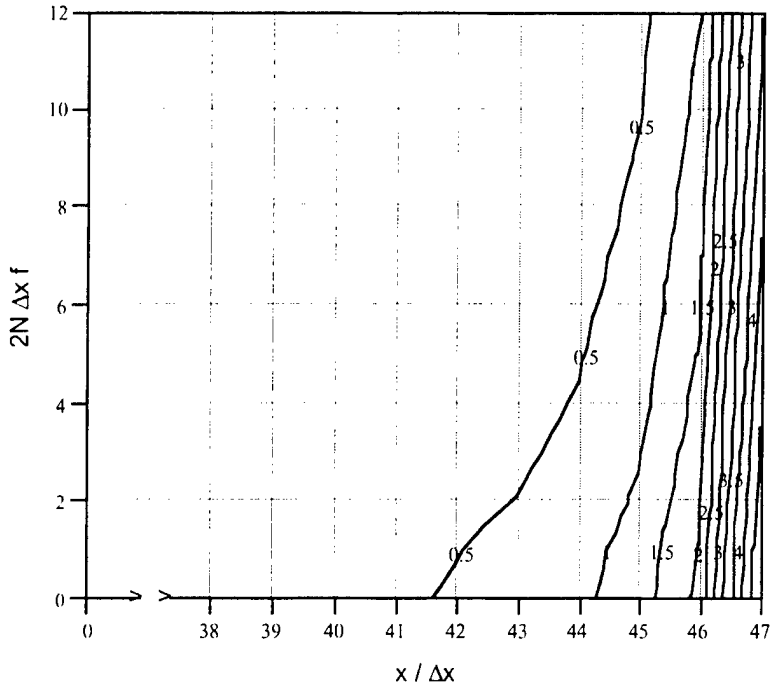

Figure 7. Transfer function of edge effect error for kernel (41).

9. Numerical Example

The circular convolution error, ε_1, given by (32), and the edge effect, ε_{edge}, given by (34), were calculated from a regular grid of equal-area mean gravity anomalies convolved with the kernel (41). This convolution yields the vertical gravity anomaly gradient, given in planar approximation by

$$\frac{\partial \Delta g}{\partial z}(x,y) = \frac{1}{2\pi} \int_{-\infty}^{\infty}\int_{-\infty}^{\infty} \frac{\Delta g(x',y') - \Delta g(x,y)}{\left((x-x')^2 + (y-y')^2\right)^{3/2}}\, dx'\, dy' \qquad (42)$$

The total data array is a grid of $2\,N_1 = 680$ by $2\,N_2 = 540$ values in the west-midwest part of the United States. The grid mesh size is 4 km by 4 km. The circular convolution errors and edge effects were computed for the inner $N_1 \times N_2$ area and are shown in Figures 8 and 9, respectively. As predicted by the error transfer functions (Figures 6 and 7), the errors are largest near the edges of this computation area. The most inner $N_1/2 \times N_2/2$ area shown in Figures 8 and 9 by dotted lines indicates the area that might be considered free of edge effects (although it could be larger).

In Table 3, the root-mean-square (rms) errors are listed for each type of error and for each region, inside and outside the dotted lines. It is clear from the figures and the table that the circular convolution error and the edge effect are commensurate. Avoiding the latter, which must be done in any case, also avoids the former, and no zero-padding of the data is needed.

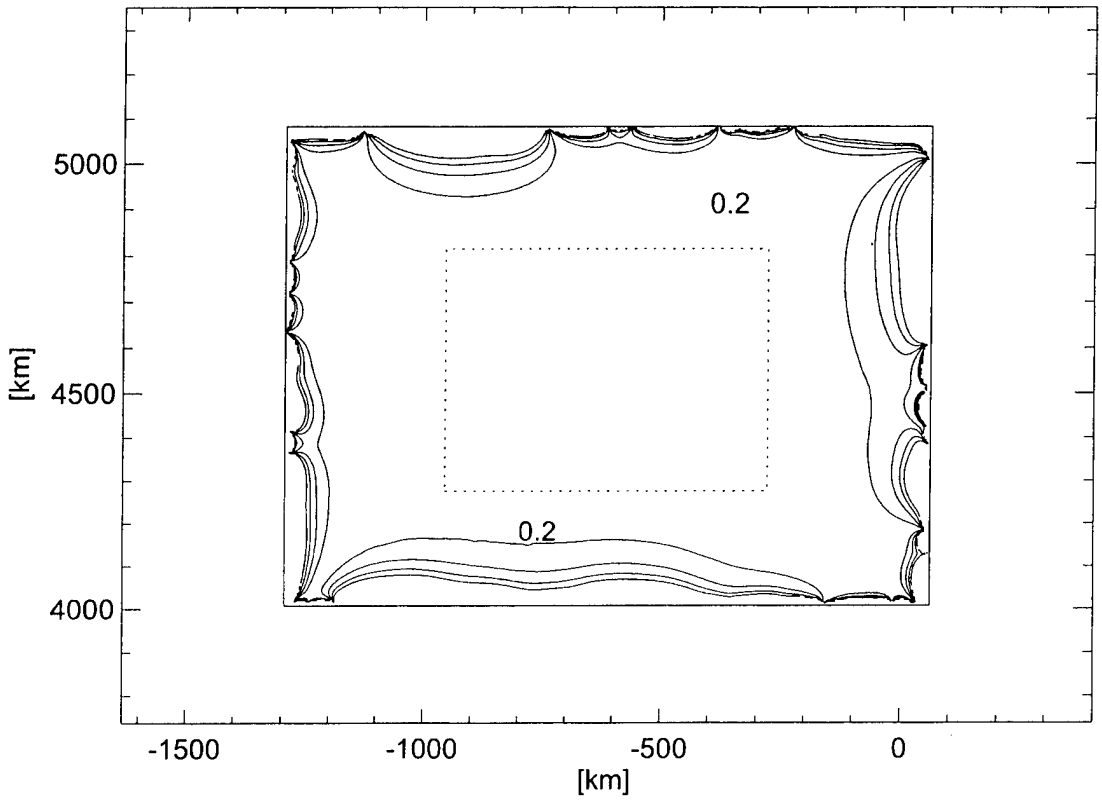

Figure 8. Circular convolution errors (absolute values) for the vertical gradient of the gravity anomaly. The contours decrease in value from the edges with interval equal to 0.2 Eötvös.

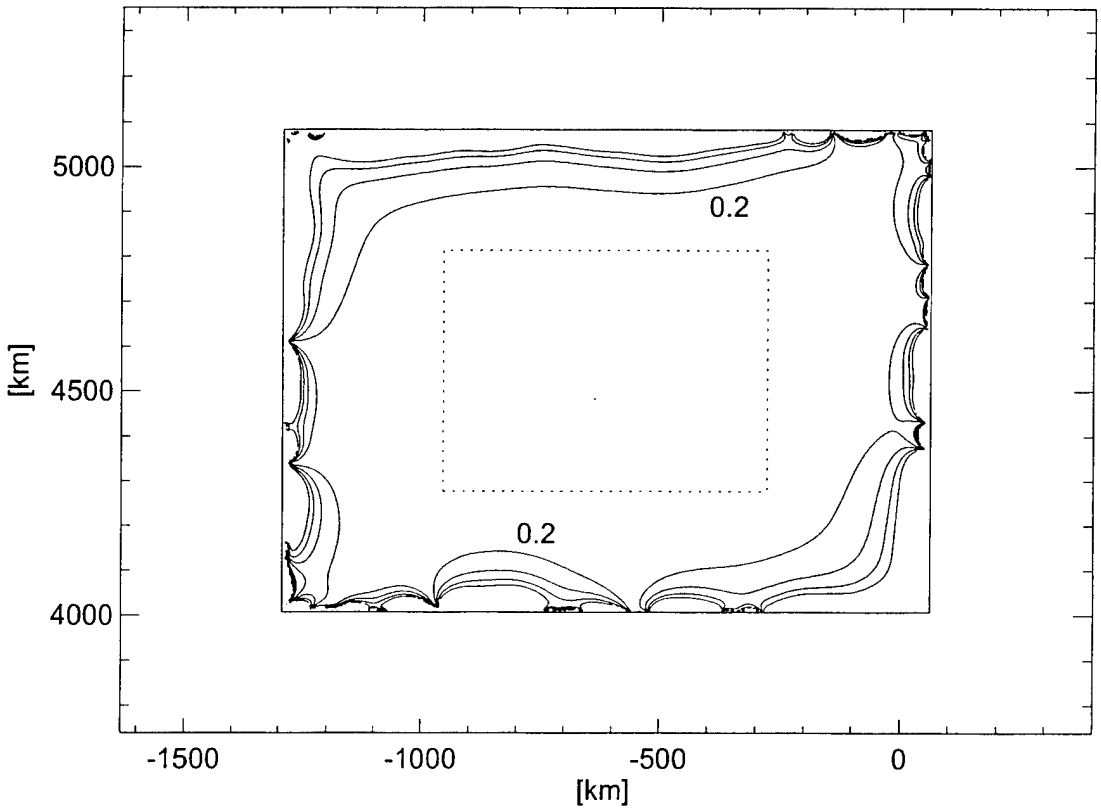

Figure 9. Edge effect (absolute values) for the vertical gradient of the gravity anomaly. The contours decrease in value from the edges with interval equal to 0.2 Eötvös.

Table 3: RMS values of the circular convolution error, edge effect, and their sum for the example of the vertical gravity anomaly gradient described in the text. Units are Eötvös. Areas are delineated by the dotted lines in Figures 8 and 9.

	Edge Effect	Circ. Conv. Err.	Total
RMS of Inner Area	0.023	0.027	0.034
RMS of Outer Area	4.478	4.434	6.116
Abs. Max. Err.	135.2	129.4	167.3

10. Derivatives

Derivatives of signals, and of convolutions, play an important role in geodesy. For example, consider the deflection of the vertical according to the Vening-Meinesz formula, that is the

derivative of Stokes' formula, that, in turn, is a convolution of gravity anomalies and Stokes' function. As another (rather arcane) example, the terrain correction is the vertical gravitational attraction at a point P due to the mass attraction of the residual topography, $\Delta b = b_P - b_Q$, with respect to point P. In planar approximation, it is given by a series of iterated convolutions (Sideris, 1990). Klose and Ilk (1993) give the correct formulation of the attraction in terms of Fourier transforms:

$$A(P) = k\rho \sum_{r=1}^{\infty} A_r(P) \tag{43}$$

where k is Newton's gravitational constant, ρ is the (constant) density of topographic mass, and

$$A_r(P) = \frac{(2\pi)^{2r}}{(2r)!} \sum_{n=0}^{2r-1} (-1)^n \binom{2r}{n} \left[F^{-1}\left(F\left(b_Q^{2r-n} \right) f^{2r-1} \right) \right]_P b_P^n \tag{44}$$

where $F(\cdot)$ denotes continuous Fourier transform, and f is frequency given by

$$f = \sqrt{f_1^2 + f_2^2} \tag{45}$$

The factors f^{2r-1} have a conventional (though not required) interpretation (Sideris, 1990) as being due to vertical derivative operators applied to the residual topography, formally extended harmonically into exterior space like a potential.

Finally, having computed the terrain effect according to (43) (or some approximate convolution), it is possible using standard properties of the Fourier transform to calculate derivatives of the attraction, thus yielding terrain effects for the gravitational gradients. It is first noted that from the relationship between A(P) and the corresponding generating potential, T, that is, $A(P) = -\partial T(P)/\partial Z$, we obtain

$$F(T) = \frac{1}{2\pi f} F(A) \tag{46}$$

Then, the second-order gradients of the potential can be expressed formally as (see also Tziavos et al., 1988)

$$\Gamma_{x_n x_m} = \frac{\partial^2 T}{\partial x_n \partial x_m} = F^{-1}\left(\frac{(i\,2\pi f_n)(i\,2\pi f_m)}{2\pi f} F(A) \right); \quad n = 1,2 \; ; \; m = 1,2 \tag{47}$$

$$\Gamma_{x_n z} = \frac{\partial^2 T}{\partial x_n \partial z} = -F^{-1}\left((i\,2\pi f_n) F(A) \right); \quad n = 1,2 \tag{48}$$

$$\Gamma_{z,z} = \frac{\partial^2 T}{\partial z^2} = - F^{-1}\left((2\pi f)\, F(A) \right) \tag{49}$$

In each of the cases listed, (44), (47), (48), (49), and others, the desired quantity is the inverse transform of the product of a two functions of frequency, one representing a signal and the other representing derivative operators. Thus, according to the convolution theorem, the desired quantity is a convolution - but only formally in these cases since the derivative operators must then be viewed as derivatives of the Dirac delta function. When approximating these continuous "convolutions" with cyclic, discrete convolutions (amenable to FFT processing), where, furthermore, $F(A)$ may be already approximated by a cyclic, discrete convolution, it is important to define properly the discrete versions of the derivative operator "transforms", such as $(i\, 2\pi\, f_n)$ in equation (48).

Since the signal being differentiated is assumed to be real, the result of the cyclic, discrete convolution with the derivative operator should also be real. Therefore, the DFT of the signal and the DFT of this convolution both satisfy the conjugate symmetry property (cf. (5)), which means the DFT of the derivative operator should also satisfy the conjugate symmetry property. For two dimensional periodic discrete sequences defined over the fundamental area,

$$-N_1/2 \le \ell_1 \le N_1/2 - 1\,, \quad -N_2/2 \le \ell_2 \le N_2/2 - 1 \tag{50}$$

the conjugate symmetry property is

$$\left(\tilde{H}_{N_1,N_2}\right)_{-\ell_1,\ell_2} = \left(\tilde{H}^{*}_{N_1,N_2}\right)_{\ell_1,-\ell_2} \tag{51}$$

The necessary condition (51) and periodicity of the discrete spectrum imply that four spectral values must be real:

$$\begin{gathered} \left(\tilde{H}_{N_1,N_2}\right)_{0,0} = \left(\tilde{H}^{*}_{N_1,N_2}\right)_{0,0}; \qquad \left(\tilde{H}_{N_1,N_2}\right)_{0,-N_2/2} = \left(\tilde{H}^{*}_{N_1,N_2}\right)_{0,-N_2/2} \\ \left(\tilde{H}_{N_1,N_2}\right)_{-N_1/2,0} = \left(\tilde{H}^{*}_{N_1,N_2}\right)_{-N_1/2,0}; \quad \left(\tilde{H}_{N_1,N_2}\right)_{-N_1/2,-N_2/2} = \left(\tilde{H}^{*}_{N_1,N_2}\right)_{-N_1/2,-N_2/2} \end{gathered} \tag{52}$$

In addition, there is conjugate symmetry in ℓ_1 for $\ell_2 = 0$ and $\ell_2 = -N_2/2$:

$$\left(\tilde{H}_{N_1,N_2}\right)_{-\ell_1,0} = \left(\tilde{H}^{*}_{N_1,N_2}\right)_{\ell_1,0}; \quad \left(\tilde{H}_{N_1,N_2}\right)_{-\ell_1,-N_2/2} = \left(\tilde{H}^{*}_{N_1,N_2}\right)_{\ell_1,-N_2/2} \tag{53}$$

and in ℓ_2 for $\ell_1 = 0$ and $\ell_1 = -N_1/2$:

$$\left(\tilde{H}_{N_1,N_2}\right)_{0,\ell_2} = \left(\tilde{H}^{*}_{N_1,N_2}\right)_{0,-\ell_2}\,; \quad \left(\tilde{H}_{N_1,N_2}\right)_{-N_1/2,\ell_2} = \left(\tilde{H}^{*}_{N_1,N_2}\right)_{-N_1/2,-\ell_2} \tag{54}$$

Thus, given the discretization of the derivative operator transform for the frequencies (52), one must ensure that symmetries (51), (52), (53), and (54) are fulfilled. This is *not* automatic, for example, in the case of $(i\,2\pi\,f_n)$, and one must override the continuous definition with the discrete symmetries. Then, for FFT processing, the resulting transform may be translated by periodicity to the domain $0 \le \ell_1 \le N_1 - 1$, $0 \le \ell_2 \le N_2 - 1$ using a procedure analogous to (28).

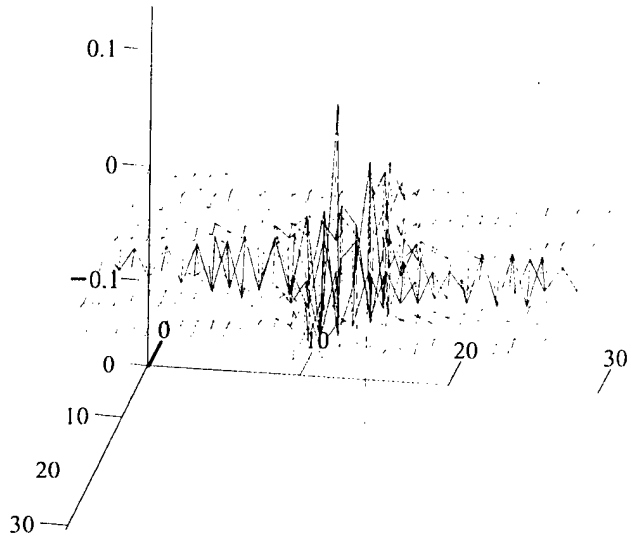

Fig. 10. Discrete kernel of the derivative operator $\partial^2/(\partial x_1\,\partial x_2)$ $(N_1 = N_2 = 32)$.

As one might expect, the cyclic convolution errors are significant only for computation points close to the edge of the computation area. Furthermore, because of the ripple effect, the error dominates in the high frequency domain. Again, to avoid the cyclic convolution error one should extend the signal with zeros, as in (25) or (27). On the other hand, the edge effect remains, and will be of the same order of magnitude as the cyclic convolution error if the signal is not extended. If the derivative operator transform multiplies a convolution transform, as in (47) - (49), and it is a cyclic convolution operating on extended (padded) arrays, then the derivative transform should be extended, as well, and should be padded with its own natural values according to the symmetry properties (51) - (54).

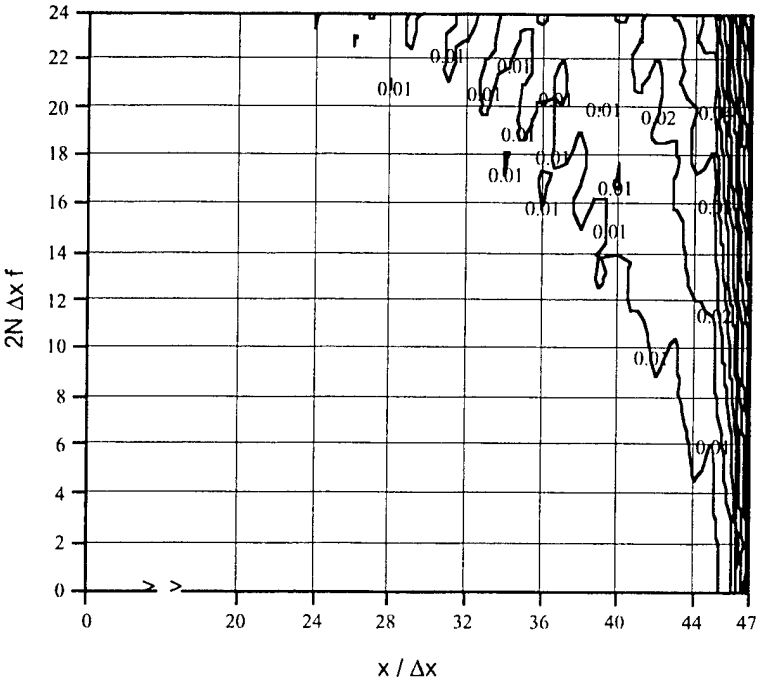

Fig. 11. Transfer function of cyclic convolution error ε_1 for the kernel of Figure 10.

11. Summary

The methods of approximating a convolution by a discrete, cyclic convolution (for FFT implementation) in the past have been studied empirically as applied to geodetic problems. Various techniques were tested on actual data by numerous investigators to determine, in some probabilistic sense, the accuracy of the methods.

The results of the present discussion are three-fold. Expressions are derived for the discrete circular convolution error, for the error committed by improper zero-padding of the kernel sequence, and for the edge effect (discrete approximation). Second, through the use of error transfer functions and a numerical example, it is shown that the cyclic convolution error committed by *not* extending the arrays is not greater than the error associated with the edge effect. Therefore, by limiting the computational area to reduce the edge effect (that does not disappear with extensions), one automatically reduces by similar amount the cyclic convolution error. This is important when convolving large arrays, and extensions (quadrupling memory requirements) are not feasible. A by-product of the analysis is that extending the kernel with zeros makes no sense from an accuracy viewpoint, although the error is less than with no extensions. And third, the analysis is extended to properly defined discrete derivative operator transforms with a demonstration through error transfer functions that the resulting cyclic convolution error is confined to the high frequencies and to computation points very close to the edge, as expected.

Acknowledgments. The author thanks reviewers M.G. Sideris and W.D. Schuh for many valuable comments. This work was supported by a research project funded by the National Imagery and Mapping Agency (NIMA) and administered by the U.S. Air Force Phillips Laboratory under contract no. F19628-94-K-0005, OSU Research Foundation project no.730155.

References

Haagmans R, de Min E, van Gelderen M (1993) Fast evaluation of convolution integrals on the sphere using 1D FFT, and a comparison with existing methods for Stokes' integral. *Manuscripta Geodaetica*, 18(5), 227-241.

Klose U, Ilk KH (1993) A solution to the singularity problem occurring in the terrain correction formula. *Manuscripta Geodaetica*, 18, 263-279.

Oppenheim AV, Schafer RW (1975) Digital Signal Processing. Prentice-Hall, Inc., Englewood Cliffs, New Jersey.

Schwarz KP, Sideris MG, Forsberg R (1990) The use of FFT techniques in physical geodesy, *Geophys. J. Int.*, 100, 485-514.

Sideris MG 1990 Rigorous gravimetric terrain modelling using Molodensky's operator. *Manuscripta Geodaetica*, 15, 97-106.

Sideris MG, Li YC (1993) Gravity field convolutions without windowing and edge effects. *Bulletin Géodésique*, 67(2), 107-118.

Tziavos IN (1992) Alternative numerical techniques for the efficient computation of terrain corrections and geoid undulations. Proc. First Continental Workshop on the Geoid in Europe, Prague, May 11-14, 1992, published by Research Institute of Geodesy, Topography and Cartography, Prague, in cooperation with IAG Subcommission For the Geoid in Europe.

Tziavos IN (1996) Comparisons of spectral techniques for geoid computations over large regions. Journal of Geodesy, 70(6), 357-373.

Tziavos IN, Sideris MG, Forsberg R, Schwarz KP (1988) The effect of the terrain on airborne gravity and gradiometry. *Journal of Geophysical Research*, 93(B8), 9173-9186.

Vermeer M (1995) Mass point geopotential modelling using fast spectral techniques: historical overview, toolbox description, numerical experiment. Manuscripta Geodaetica, 20(5), 362-378.

Zhang C (1995) A general formula and its inverse formula for gravimetric transformations by use of convolution and deconvolution techniques. Journal of Geodesy, 70(1-2), 51-64.